# Excitation of high-frequency in-plane bulk acoustic resonance modes in geometrically engineered hafnium zirconium oxide nanoelectro-mechanical membrane

Cite as: Appl. Phys. Lett. **117**, 063502 (2020); https://doi.org/10.1063/5.0016347 Submitted: 03 June 2020 . Accepted: 03 August 2020 . Published Online: 13 August 2020

厄 F. Hakim, 厄 M. Ghatge, and 厄 R. Tabrizian

# **COLLECTIONS**

Paper published as part of the special topic on Ferroelectricity in Hafnium Oxide: Materials and Devices FEHO2021







# **ARTICLES YOU MAY BE INTERESTED IN**

Study of ferroelectric characteristics of  $Hf_{0.5}Zr_{0.5}O_2$  thin films grown on sputtered or atomic-layer-deposited TiN bottom electrodes

Applied Physics Letters 117, 022902 (2020); https://doi.org/10.1063/5.0011663

The electrocaloric effect in doped hafnium oxide: Comparison of direct and indirect measurements

Applied Physics Letters 117, 042903 (2020); https://doi.org/10.1063/5.0012746

Ferroelectricity in hafnium oxide thin films

Applied Physics Letters 99, 102903 (2011); https://doi.org/10.1063/1.3634052



# Your Qubits. Measured.

Meet the next generation of quantum analyzers

- Readout for up to 64 qubits
- Operation at up to 8.5 GHz, mixer-calibration-free
- Signal optimization with minimal latency





# **Excitation of high-frequency in-plane bulk** acoustic resonance modes in geometrically engineered hafnium zirconium oxide nano-electro-mechanical membrane

Cite as: Appl. Phys. Lett. 117, 063502 (2020); doi: 10.1063/5.0016347 Submitted: 3 June 2020 · Accepted: 3 August 2020 ·







Published Online: 13 August 2020

F. Hakim, (D) M. Ghatge, (D) and R. Tabrizian<sup>a)</sup> (D)



## **AFFILIATIONS**

Department of Electrical and Computer Engineering, University of Florida, Gainesville, Florida 32611, USA

Note: This paper is part of the Special Topic on Materials and Devices Utilizing Ferroelectricity in Halfnium Oxide. <sup>a)</sup>Author to whom correspondence should be addressed: rtabrizian@ufl.edu

### **ABSTRACT**

A nano-electro-mechanical membrane created from atomic-layered ferroelectric hafnium zirconium oxide (Hf<sub>0.5</sub>Zr<sub>0.5</sub>O<sub>2</sub>), titanium nitride (TiN), and silicon dioxide is engineered to localize high quality factor (Q) in-plane bulk acoustic resonance modes over 80-840 MHz. The in-plane geometry of the membrane, with an overall thickness of 50 nm and an aspect ratio exceeding 104:1, is optimized to simultaneously preserve the stress profile needed for sustaining ferroelectric polarization and enable propagation and constructive interaction of extensional and shear waves to create bulk acoustic modes. A ferroelectric polarization of 11.2  $\mu$ C/cm<sup>2</sup> is measured at the transduction ports, which is consistent after nano-membrane release. The first, third, and seventh order width extensional modes (WE<sub>1,3,7</sub>) and the third order of the width shear mode (WS<sub>3</sub>) are electrically measured at 109, 389, 766, and 267 MHz, respectively, showing Qs over 50-100 that are dominated by the large electrical resistance of TiN electrodes. High mechanical Qs of 538, 407, 781, and 594 are extracted for the WE<sub>1,3,7</sub> and WS<sub>3</sub> modes, respectively, after de-embedding the TiN electrode impedance, resulting in large resonance frequency  $(f_0) \times Q$  products as high as  $6 \times 10^{11}$ . The measured characteristics, along with numerical simulations, are used to extract a Young's modulus of  $\sim 340\,\mathrm{GPa}$  for the 10 nm-thick Hf<sub>0.5</sub>Zr<sub>0.5</sub>O<sub>2</sub> film, which is in close agreement with the reported ab initio estimations.

Published under license by AIP Publishing. https://doi.org/10.1063/5.0016347

The recent demonstration of nano-electro-mechanical transducers based on ferroelectric hafnium zirconium oxide (Hf<sub>0.5</sub>Zr<sub>0.5</sub>O<sub>2</sub>) augurs realization of integrated sensors, actuators, and resonators at the nanoscale.<sup>1-5</sup> Among its various transforming applications, the atomic-layered Hf<sub>0.5</sub>Zr<sub>0.5</sub>O<sub>2</sub> transducer provides unique characteristics that enable integration of high-performance nano-acoustic resonators and filters operating over a wide frequency spectrum. 1,4,5 Unlike any other ferroelectric film, Hf<sub>0.5</sub>Zr<sub>0.5</sub>O<sub>2</sub> sustains a large polarization and coercive field when scaled to few nanometers thickness.<sup>6–8</sup> This facilitates creation of super-high frequency resonators with low-impedance and extended dynamic range of linear operation: two essential metrics needed for acoustic spectral processors to serve in radio frequency (RF) front-end modules.

Realization of high frequency and high quality-factor (Q) acoustic resonators requires excitation and energy confinement of laterally polarized extensional and shear acoustic waves in atomically thin Hf<sub>0.5</sub>Zr<sub>0.5</sub>O<sub>2</sub> membranes. 10,11 Unlike flexural waves, as the membrane thickness is extremely scaled to a few nanometers, the propagation velocity of the in-plane extensional and shear waves remains high, nearly independent from the membrane thickness. Proper localization of such waves results in highfrequency bulk acoustic resonance modes with several orders of magnitude higher frequency compared to flexural modes. 12 Furthermore, bulk acoustic modes benefit from a large volume to surface mechanical energy distribution ratio that is essential to achieve high electromechanical transduction coupling in piezoelectric and ferroelectric mechanical resonators.<sup>1</sup>

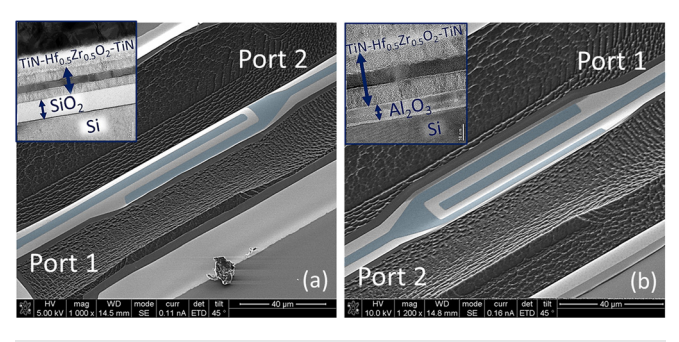
However, harnessing the advantages of bulk acoustic modes requires creation of perfectly flat membranes. <sup>12</sup> Even a slight curvature in the membrane results in the scattering of laterally propagating extensional and shear waves, which prevents from their constructive interaction that is needed to form a resonance mode. 14

Considering the large planar transduction area needed to achieve low motional impedance for RF applications, excitation of bulk acoustic resonance modes in  $Hf_{0.5}Zr_{0.5}O_2$  nano-membranes requires sustaining a flat geometry with an aspect ratio exceeding  $10^4$ :1. This is particularly challenging, considering the large internal stress in atomically engineered  $Hf_{0.5}Zr_{0.5}O_2$  that is the basis to preserve the orthorhombic morphology and ferroelectric behavior. <sup>15,16</sup>

In this work, we demonstrate the effect of stress relaxation in released  $Hf_{0.5}Zr_{0.5}O_2$  nano-membranes and present engineering approaches to sustain ferroelectric and geometrical characteristics needed for excitation of high frequency bulk acoustic modes. A nanomembrane resonator prototype is presented with in-plane extensional and shear resonance modes over 80–840 MHz with large Qs. This first demonstration of high frequency and high Q bulk acoustic resonance modes in  $Hf_{0.5}Zr_{0.5}O_2$  nano-membranes also enables a first-hand experimental extraction of the Young's modules of the ferroelectric  $Hf_{0.5}Zr_{0.5}O_2$  film.

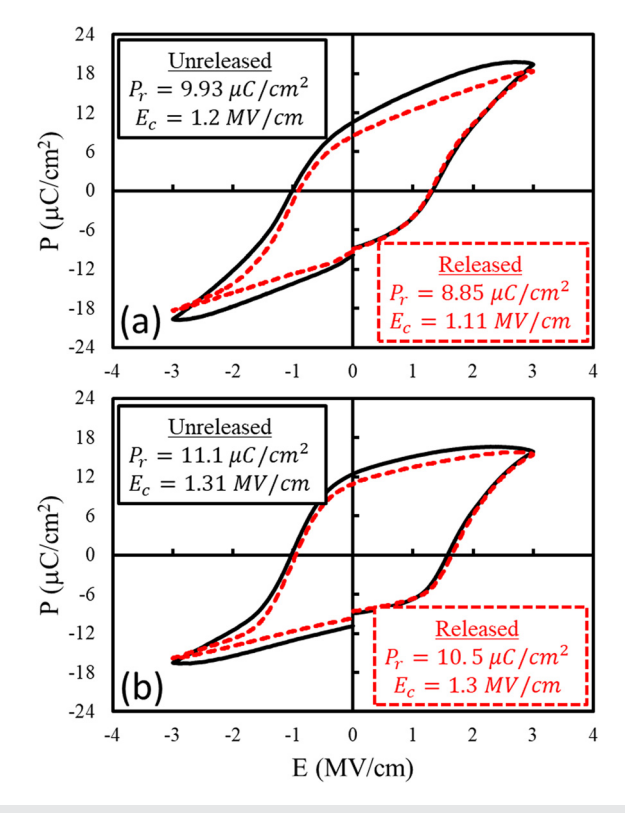
The nano-membrane resonators presented in this article are created from atomic layer deposition (ALD) and patterning of 10 nmthick Hf<sub>0.5</sub>Zr<sub>0.5</sub>O<sub>2</sub> and titanium nitride (TiN) layers, a top of (100) silicon substrate that is covered by a dielectric spacer. ALD 25 nmthick silicon dioxide (SiO<sub>2</sub>) and 10 nm-thick alumina (Al<sub>2</sub>O<sub>3</sub>) are used in different samples as the spacer, not only to protect the TiN-Hf<sub>0.5</sub>Zr<sub>0.5</sub>O<sub>2</sub>-TiN transducer during the membrane release but also to enable exploration of the effect of the structural layer material on the transducer characteristics. The fabrication process for realization of a Hf<sub>0.5</sub>Zr<sub>0.5</sub>O<sub>2</sub>-based nano-electro-mechanical resonators is composed of three major steps that are ALD19 and rapid thermal annealing (RTA) of the transducer stack to promote non-centrosymmetric orthorhombic phase, 6-8 selective patterning of TiN layers to create electrically isolated transduction ports, 1,4,5,8 and releasing the high aspect-ratio nano-membranes from the substrate to create the acoustic cavity. Ideally, the fabrication process should preserve the ferroelectric characteristics of the Hf<sub>0.5</sub>Zr<sub>0.5</sub>O<sub>2</sub> transducer and ensure creation of a sufficiently flat nano-membrane geometry. In practice, the large residual stress in the atomically engineered Hf<sub>0.5</sub>Zr<sub>0.5</sub>O<sub>2</sub> film results in undesirable warping of the nano-membrane upon release that not only prevents formation of in-plane extensional modes but also degrades the ferroelectric characteristic of the transducer and its corresponding electromechanical coupling efficiency. 4,1

Figure 1 shows the SEM image of two convex nano-membrane transducers implemented on SiO<sub>2</sub> and Al<sub>2</sub>O<sub>3</sub> spacers, where a



**FIG. 1.** SEM image of convex  $Hf_{0.5}Zr_{0.5}O_2$  nano-membrane resonators on (a)  $SiO_2$  and (b)  $Al_2O_3$  spacers, highlighting their bending after release.

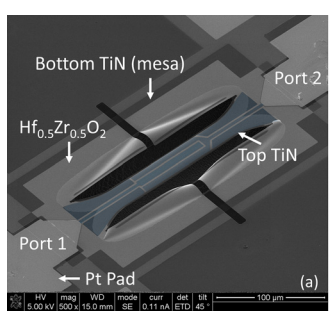
significant distortion in the flat geometry is observed in both cases. The residual stress in the stack is a natural result of the thermomechanical engineering of the Hf<sub>0.5</sub>Zr<sub>0.5</sub>O<sub>2</sub> film that is needed to enable the morphological transition to the preferred orthorhombic phase. 15,16 Such a transition follows a complicated path starting from monoclinic to tetragonal phase transformation during temperature ramp up in RTA, and from tetragonal to orthorhombic phase during the cooling followed by the RTA, and leaves a complex stress profile in the film. 15,20 When the nano-membrane is released through etching the silicon cavity, the residual stress forces transformation of the geometry according to the relative elastic stiffness of the constituent layers in the stack. In the Hf<sub>0.5</sub>Zr<sub>0.5</sub>O<sub>2</sub>-on-SiO<sub>2</sub> case, the larger elastic constant of the Hf<sub>0.5</sub>Zr<sub>0.5</sub>O<sub>2</sub> results in relaxation of the stress in Hf<sub>0.5</sub>Zr<sub>0.5</sub>O<sub>2</sub> and buckles the nano-membrane downwards [Fig. 1(a)]. On the other hand, in Hf<sub>0.5</sub>Zr<sub>0.5</sub>O<sub>2</sub>-on-Al<sub>2</sub>O<sub>3</sub>, the dominant Al<sub>2</sub>O<sub>3</sub> stiffness induces further compressional stress in the Hf<sub>0.5</sub>Zr<sub>0.5</sub>O<sub>2</sub> film and buckles the nano-membrane upwards. Aside from the geometrical transformation, the substantial change in the surface boundary condition induced upon release of the nano-membrane induces a large change in stress profile, which may translate to a partial change in the morphological content of the  $Hf_{0.5}Zr_{0.5}O_2$  film. Figure 2 compares the measured polarization-electric field (PE) hysteresis loop of the Hf<sub>0.5</sub>Zr<sub>0.5</sub>O<sub>2</sub>-on-SiO<sub>2</sub> and Hf<sub>0.5</sub>Zr<sub>0.5</sub>O<sub>2</sub>-on-Al<sub>2</sub>O<sub>3</sub> transducers, before and after release. The relaxation of the stress in the released Hf<sub>0.5</sub>Zr<sub>0.5</sub>O<sub>2</sub>-on-SiO<sub>2</sub> nano-membrane results in significant degradation of the remanent



**FIG. 2.** The polarization-electric field (PE) hysteresis loop of the transducer, measured at the port 1, for the (a)  $Hf_{0.5}Zr_{0.5}O_2$ -on- $SiO_2$  and (b)  $Hf_{0.5}Zr_{0.5}O_2$ -on- $Al_2O_3$  nano-membranes, measured before and after release.

polarization. The decrease in remanent polarization is attributed to the partial reversion of orthorhombic domains back to the tetragonal phase.  $^{15,16}$  An increase in the remanent-state dielectric constant from 29 to 41 further supports this hypothesis. On the other hand, in the  $Hf_{0.5}Zr_{0.5}O_2$ -on-Al $_2O_3$  sample, the polarization remains nearly the same, which can be attributed to the large elastic constant of the 10 nm-thick Al $_2O_3$  that sustain the stress profile in the  $Hf_{0.5}Zr_{0.5}O_2$  film after nano-membrane release. The upward buckling of the  $Hf_{0.5}Zr_{0.5}O_2$ -on-Al $_2O_3$  nano-membrane [Fig. 1(b)] supports this hypothesis.

While the buckling of the released nano-membrane affects the ferroelectric properties of the transducer, it substantially disperses extensional and shear acoustic excitations.<sup>14</sup> In this work, to sustain the geometrical flatness after the release and enable high-Q energy localization of bulk acoustic modes, the lateral geometry of the nanomembrane is engineered. A concave geometry with wide anchoring tethers is used to compensate the effect of the nano-membrane release on the transducers stress profile. Figure 3 shows the SEM images of the concave and convex Hf<sub>0.5</sub>Zr<sub>0.5</sub>O<sub>2</sub>-on-SiO<sub>2</sub> nano-membrane resonators. The substantial increase in the flexural stiffness in the concave geometry [Fig. 3(a)] prevents from nano-membrane buckling after release. Furthermore, the gradual increase in the nano-membrane width, as moving toward the flanks, preserves the stress profile in the central region, which is needed to sustain the ferroelectric characteristics of the transducer. 15,16 Finally, optimization of the concave curvature, using dispersion engineering techniques, 10 enables localization of the extensional or shear excitations in the central region of the nanomembrane and creation of high-Q bulk acoustic modes. Figure 4(a) compares the measured PE hysteresis loop of the released concave and convex Hf<sub>0.5</sub>Zr<sub>0.5</sub>O<sub>2</sub>-on-SiO<sub>2</sub> nano-membranes, with a similar central width, length, and electrode configuration. Unlike the convex counterpart, the remanent polarization remains unchanged in the concave nano-membrane after release. Figure 4(b) compares the relative dielectric-constant hysteresis loop of the released Hf<sub>0.5</sub>Zr<sub>0.5</sub>O<sub>2</sub>-on-SiO<sub>2</sub> nano-membranes with concave and convex geometries. A significantly higher maximum dielectric-constant, measured at the coercive field, is evident in the concave nano-membrane and is attributed to a



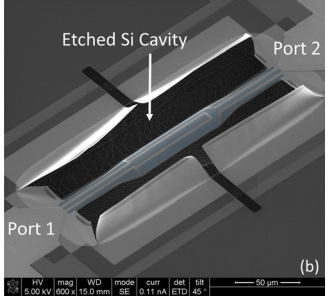


**FIG. 3.** The SEM image of the (a) geometrically engineered concave and (b) convex two-port  $Hf_{0.5}Zr_{0.5}O_2$ -on-SiO<sub>2</sub> nano-membrane resonator. The concave geometry enables preserving the ferroelectric characteristics of the transducer after release from the substrate. It also sustains the flatness of the nano-membrane and enables excitation of high velocity extensional and shear waves to create high frequency bulk acoustic modes. The TiN transducer electrodes, defining the two ports of the resonator, and the dummy electrodes, placed to maintain the continuity of acoustic impedance, are highlighted on the images.

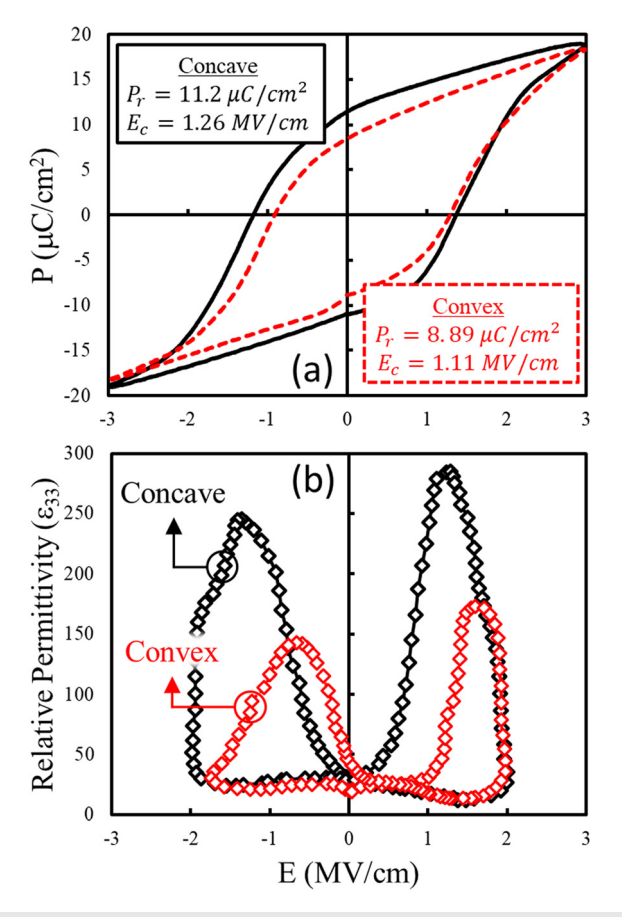


**FIG. 4.** (a) The measured (a) PE and (b) dielectric-constant hysteresis characteristic of the concave and convex  $Hf_{0.5}Zr_{0.5}O_2$ -on-SiO<sub>2</sub> nano-membrane resonators.

substantial increase in the efficiency of the polarization switching process. <sup>17,18</sup> This increase is enabled by the flat geometry of the concave nano-membrane that supports the propagation of domain-wall motion during polarization switching, by fast guided waves.

The frequency response of the two-port concave Hf<sub>0.5</sub>Zr<sub>0.5</sub>O<sub>2</sub>on-SiO<sub>2</sub> nano-membrane resonator is measured using a Keysight N5222A Vector Network Analyzer (VNA). Prior to the RF measurements, a DC polarization voltage of  $\sim 3 \, \mathrm{V}$  is applied to the transducer, to ensure operation in the polarized state. Figure 5 shows the forward transmission response (i.e., S<sub>21</sub>) of the concave Hf<sub>0.5</sub>Zr<sub>0.5</sub>O<sub>2</sub>-on-SiO<sub>2</sub> nano-membrane resonator over 80-840 MHz span, highlighting various resonance peaks at 109, 267, 389, and 766 MHz, with Qs of 49, 54, 37, and 71, respectively. A COMSOL simulation model is developed, based on the use of ab initio material properties of the ferroelectric Hf<sub>0.5</sub>Zr<sub>0.5</sub>O<sub>2</sub> film, <sup>21,22</sup> to identify the vibration mode-shapes corresponding to the measured resonance peaks. The simulated frequency and vibration mode-shapes of the first, third, and seventh width-extensional (WE<sub>1,3,7</sub>) and the third width-shear (WS<sub>3</sub>) modes are shown in Fig. 5, highlighting a close match with the peaks in the measured transmission response. The 109 MHz, 389 MHz, and 766 MHz peaks are close to the WE<sub>1</sub>, WE<sub>3</sub>, and WE<sub>7</sub> modes, respectively, and the 267 MHz peak is close to the WS<sub>3</sub> mode. Parametric variation

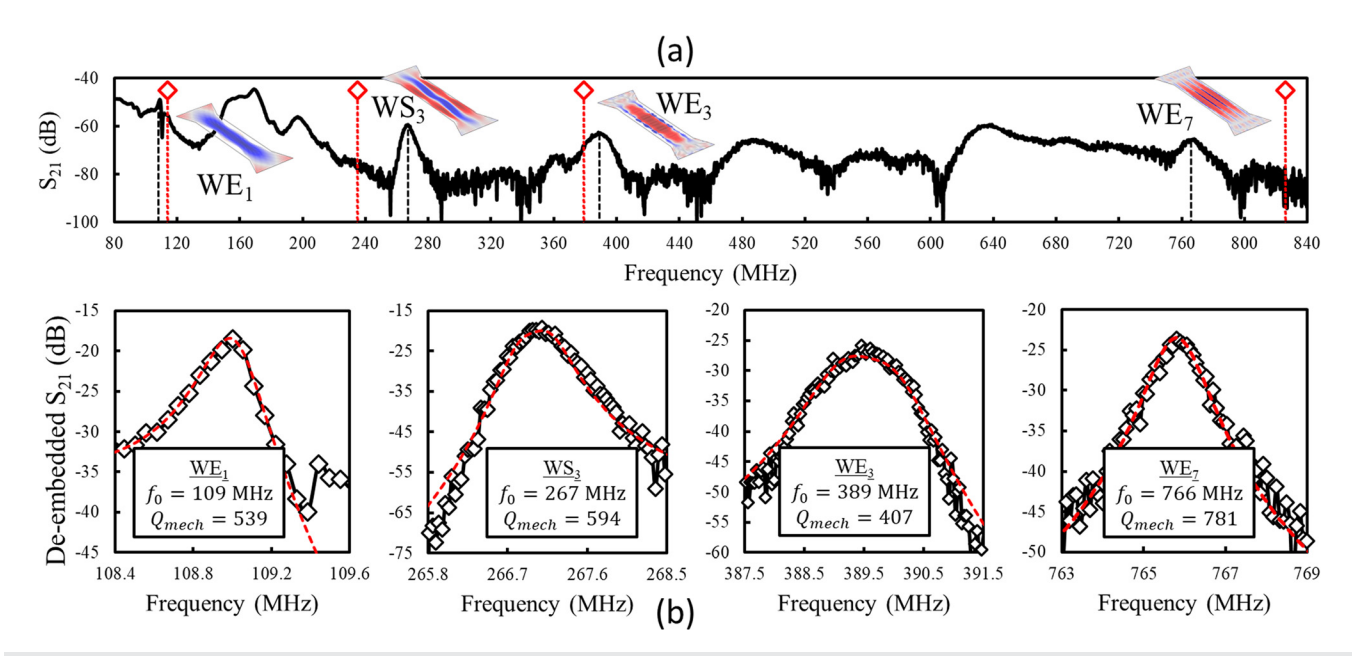


FIG. 5. (a) The large-span forward transmission response of the concave Hf<sub>0.5</sub>Zr<sub>0.5</sub>O<sub>2</sub>-on-SiO<sub>2</sub> nano-membrane resonator. The bulk acoustic vibration mode shapes and their corresponding simulated frequencies (in dashed red lines) are also shown. (b) The short-span response at each mode, after de-embedding the TiN electrode impedance.

of the  $Hf_{0.5}Zr_{0.5}O_2$  elastic constants is applied to match the frequency of simulated  $WE_1$  and  $WE_3$  modes with the measured values. This enables the first-hand experimental extraction of a Young's modulus of  $\sim\!340$  GPa for the 10 nm-thick ferroelectric  $Hf_{0.5}Zr_{0.5}O_2$  film, which is in close agreement with the  $\sim\!347$  GPa value calculated from the local density approximations. <sup>21,22</sup>

The low Q of the measured resonance modes is a result of the large electrical resistance of the 10 nm-thick top and bottom TiN electrodes of the transducer. A large resistivity of 120  $\mu\Omega$  · cm is measured, using a four point probe, for the 10 nm-thick TiN that translates into a series resistance of several kilo ohms, loading the motional impedance of the nano-membrane resonator and resulting in a low measured Q. To extract the mechanical Q corresponding to the measured modes, a calibration procedure is performed based on biasing the nanomembrane transducers at the coercive field, to enable the de-embedding of the large electrical loading of the TiN electrodes without affecting the motional impedance of the transducer (see the supplementary material for the detailed description of the de-embedding procedure). Figure 5(b) shows the measured short-span frequency response of the peaks after the de-embedding procedure highlighting high Qs of 539, 594, 407, and 781 for the WE1, WS3, WE3, and WE7 modes, respectively. Among these modes, the largest resonance frequency  $(f_0) \times Q$  product of  $6 \times 10^{11}$  is measured for the WE<sub>7</sub> mode at 766 MHz. The high mechanical Q of the extensional and shear bulk acoustic modes highlights the promising potential of the Hf<sub>0.5</sub>Zr<sub>0.5</sub>O<sub>2</sub>-based nano-membrane resonators for integrated RF spectral processing and frequency reference applications. However, the large loading effect of the atomically thin electrodes on the Q should be properly addressed to enable practical adaptation of the Hf<sub>0.5</sub>Zr<sub>0.5</sub>O<sub>2</sub>-based resonators in integrated microsystems.

In conclusion, this article reports on the demonstration of high frequency and high Q bulk acoustic resonance modes in atomic-layered ferroelectric  $Hf_{0.5}Zr_{0.5}O_2$  nano-membranes over the 80-840 MHz spectrum. These resonance modes are excited through geometrical engineering of a concave Hf<sub>0.5</sub>Zr<sub>0.5</sub>O<sub>2</sub>-on-SiO<sub>2</sub> nano-membrane to preserve the ferroelectric polarization and flat geometry needed for efficient electromechanical excitation of extensional and shear waves. The effect of the release process on ferroelectric characteristics of the Hf<sub>0.5</sub>Zr<sub>0.5</sub>O<sub>2</sub> transducer is studied for nano-membranes implemented on SiO2 and Al2O3 spacers. The effect of lateral geometry flatness on the polarization switching efficiency is discussed. The two-port electrical measurement of a geometrically engineered  $Hf_{0.5}Zr_{0.5}O_2$ -on-SiO<sub>2</sub> nano-membrane resonator is presented showing bulk acoustic resonance modes at 109, 267, 389, and 766 MHz. The effect of the large impedance of thin TiN electrodes on the degradation of resonator Q is discussed. The mechanical Qs over 400-800 are extracted for the bulk acoustic modes, after de-embedding the electrode resistance. Specifically, a large  $f_0 \times Q$  products of  $6 \times 10^{11}$  is reported for the WE<sub>7</sub> mode at 766 MHz.

See the supplementary material for the detailed description of the calibration and de-embedding procedures used for characterization of the nano-membrane resonators and extraction of their mechanical quality factor.

The authors would also like to thank the staffs at the Nanoscale Research Facility, University of Florida, for their help with the fabrication and characterization of devices. This work was supported by the DARPA Young Faculty Award program.

# DATA AVAILABILITY

The data that support the findings of this study are available from the corresponding author upon reasonable request.

### **REFERENCES**

- <sup>1</sup>M. Ghatge, G. Walters, T. Nishida, and R. Tabrizian, Nat. Electron. **2**(11), 506 (2019).
- <sup>2</sup>H. A. Hsain, P. Sharma, H. Yu, J. L. Jones, F. So, and J. Seidel, Appl. Phys. Lett. 113(2), 022905 (2018).
- <sup>3</sup>M. Clemens, T. Kämpfe, R. Hoffmann, S. Eßlinger, S. Kirbach, K. Kühnel, M. Czernohorsky, L. M. Eng, and W. Weinreich, "Piezoelectric response of polycrystalline silicon-doped hafnium oxide thin films determined by rapid temperature cycles." Adv. Electron. Mater. 6(3), 1901015 (2020)
- perature cycles," Adv. Electron. Mater. **6**(3), 1901015 (2020).

  <sup>4</sup>M. Ghatge, G. Walters, T. Nishida, and R. Tabrizian, Appl. Phys. Lett. **116**(4), 043501 (2020).
- <sup>5</sup>M. Ghatge, G. Walters, T. Nishida, and R. Tabrizian, IEEE Electron Device Lett. 40(5), 800 (2019).
- <sup>6</sup>J. Müller, T. S. Böscke, D. Bräuhaus, U. Schröder, U. Böttger, J. Sundqvist, P. Kücher, T. Mikolajick, and L. Frey, Appl. Phys. Lett. 99(11), 112901 (2011).
- 7J. Müller, T. S. Böscke, U. Schröder, S. Mueller, D. Bräuhaus, U. Böttger, L. Frey, and T. Mikolajick, Nano Lett. 12(8), 4318 (2012).
- <sup>8</sup>M. Ghatge, G. Walters, T. Nishida, and R. Tabrizian, "A nano-mechanical resonator with 10nm hafnium-zirconium oxide ferroelectric transducer," *IEEE International Electron Devices Meeting (IEDM)*, 1-5 December 2018, San Francisco, CA (IEEE, 2018), pp. 4.6.1–4.6.4.
- <sup>9</sup>K. M. Lakin, G. R. Kline, and K. T. McCarron, IEEE Trans. Microwave Theory Tech. 41(12), 2139 (1993).

- <sup>10</sup>M. Ghatge, M. Ramezani, and R. Tabrizian, IEEE Trans. Ultrason., Ferroelectr., Freq. Control 66(6), 1149 (2019).
- <sup>11</sup>M. Ghatge and R. Tabrizian, IEEE Trans. Ultrason., Ferroelectr., Freq. Control 66(6), 1140 (2019).
- <sup>12</sup>J. Achenbach, Wave Propagation in Elastic Solids (Elsevier, 2012).
- 13J. Rosenbaum, Bulk Acoustic Wave Theory and Devices (Artech House on Demand, 1988).
- <sup>14</sup>L. Sorenson, P. Shao, and F. Ayazi, J. Microelectromech. Syst. 24(2), 486 (2015).
- <sup>15</sup>M. H. Park, H. J. Kim, Y. J. Kim, W. Lee, T. Moon, and C. S. Hwang, Appl. Phys. Lett. **102**(24), 242905 (2013).
- <sup>16</sup> M. H. Park, H. J. Kim, Y. J. Kim, T. Moon, and C. S. Hwang, Appl. Phys. Lett. 104(7), 072901 (2014).
- <sup>17</sup>N. Bar-Chaim, M. Brunstein, J. Grünberg, and A. Seidman, J. Appl. Phys. 45(6), 2398–2405 (1974).
- <sup>18</sup>N. Gong, X. Sun, H. Jiang, K. S. Chang-Liao, Q. Xia, and T. P. Ma, Appl. Phys. Lett. 112(26), 262903 (2018).
- <sup>19</sup>G. Walters, A. Shekhawat, S. Moghaddam, J. L. Jones, and T. Nishida, Appl. Phys. Lett. 116(3), 032901 (2020).
- <sup>20</sup>M. H. Park, H. J. Kim, Y. J. Kim, W. Lee, T. Moon, K. D. Kim, and C. S. Hwang, Appl. Phys. Lett. **105**(7), 072902 (2014).
- <sup>21</sup>R. Materlik, C. Künneth, and A. Kersch, J. Appl. Phys. 117(13), 134109 (2015).
- <sup>22</sup>R. Materlik, Doctoral dissertation, Technische Universität Dresden, 2019.